

# Topological Persistence Machine of Phase Transitions

Quoc Hoan Tran,<sup>\*</sup> Mark Chen,<sup>†</sup> and Yoshihiko Hasegawa<sup>‡</sup>

*Department of Information and Communication Engineering,  
Graduate School of Information Science and Technology,  
The University of Tokyo, Tokyo 113-8656, Japan*

(Dated: April 30, 2022)

The study of phase transitions from experimental data becomes challenging, especially when little prior knowledge of the system is available. Topological data analysis is an emerging framework for characterizing the shape of data and has recently achieved success in detecting structural transitions in material science such as glass-liquid transition. However, data obtained from physical states may not have explicit shapes as structural materials. We propose a general framework called topological persistence machine to construct the shape of data from correlations in states; hence decipher phase transitions via the qualitative changes of the shape. Our framework enables an effective and unified approach in phase transition analysis. We demonstrate the impact in highly precise detection of Berezinskii–Kosterlitz–Thouless phase transitions in classical XY model, and quantum phase transition in the transverse Ising model and Bose–Hubbard model. Intriguingly, these phase transitions have proven to be notoriously difficult in traditional methods but can be characterized in our framework without requiring prior knowledge about phases. Our approach is thus expected applicable and brings a remarkable perspective for exploring phases of experimental physical systems.

*Introduction.*— Identifying phase of matter and its transition is key to understanding many condensed-matter systems, such as anisotropic superconductors, graphene, and quantum spins with frustrations. Traditionally, the relevant local and global order parameters are calculated to classify different phases of matter. However, it is challenging to apply to systems where no conventional order parameter exists, or particularly in quantum mechanics, due to the exponentially large Hilbert space. The revolutionized machine learning approaches open new avenues in studying the phase of matter by two typical methods, namely the supervised and unsupervised methods. Supervised methods train the learning machine on samples with predefined labels of phases in well-known regimes. In contrast, unsupervised methods do not require the prior labelling but characterize the phases via dimensional reduction methods [1–3]. Both of these approaches have been found useful and succeeded in several conventional systems [4–28]. However, it remains considerable ambiguity with regard to physical interpretations and intuitive explanations [28].

Topological data analysis (TDA) [29] has emerged recently as a valuable framework based on computational topology to characterize the shape of data. The feasibility of TDA has already been demonstrated in recognizing effective structures in material science [30–36], or characterizing the behavior of dynamical systems [37–45]. Therefore, it motivates us to use TDA as a radically different but interpretable methodology to study phase transitions. TDA has also been applied to verify glass-liquid transition in material science [46], or to evaluate equilibrium phase transitions of major topological changes in the configuration space of physical systems [39]. However, for some types of systems such as quantum many-body systems, we do not have much knowledge about the configuration space due to expo-

ponential growth of the space. In these systems, only raw data from experiments or simulations of physical states are provided. These data may not simply be represented in coordinate forms to have an explicit shape to which TDA cannot be directly applied. These limitations lead us to think of a general approach to construct the shape of raw data from physical states; hence use this shape to detect phase transitions in physical systems.

In this Letter, we present the topological persistence machine based on TDA to identify the phase of matter from raw data such as bare configurations of spin states or measurements of quantum states. We first map data into a high dimensional space with a distance function defined from correlations in states. Then we focus on the topology of mapped data to extract topological features describing the shape of data. These features are relevant to topological invariants and can be used to study phases of matter. We show that our approach is universal and generally applicable to identify a variety of phases and their transitions. First, our topological features can be used to qualitatively evaluate and interpret the Berezinskii–Kosterlitz–Thouless (BKT) phase transition in XY model. We then construct an unsupervised scheme that employs the kernel method in machine learning to quantitatively detect this BKT phase transition. We also summarize the topological features into measures called topological persistence complexity. We apply these measures in well-known quantum many-body models such as transverse Ising and Bose–Hubbard models to quantify the quantum phase transition. Interestingly, only by investigating these measures for the systems with small sizes, we can estimate quantum phase transitions of extremely large systems in a high precision.

*Topological persistence machine.*— The basic idea of TDA is that topology can indicate the topological properties of a space that remain invariant under stretching

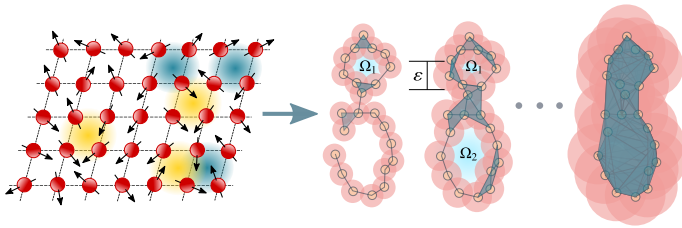


FIG. 1. Topological persistence machine takes inputs as raw data such as bare spin configurations or measurements on the physical states. Then it explores the description of the shape of data at multiple resolutions when viewing data. The data is transformed into a sequence of nested geometrical objects. Topological structure changes along this sequence are tracked, such as the merging of connected components, and the emergence and disappearance of loops present in the space.

and shrinking, such as the number of holes and the number of connected components. In particular, our topological persistence machine is based on persistent homology, which is the most used method in TDA that captures topological properties in the data at multiple scales [29, 47–49]. Here, data are not studied directly but are mapped into a set  $\mathbf{X}$  of points in a high-dimensional space associated with a distance function. To model the shape of  $\mathbf{X}$ , we place  $\varepsilon/2$ -radius balls centered at each point in  $\mathbf{X}$  to form an overlapped space  $\mathcal{T}_\varepsilon(\mathbf{X})$ . Here,  $\mathcal{T}_\varepsilon(\mathbf{X})$  is defined as the set of all points in the space within distance  $\varepsilon/2$  from some point in  $\mathbf{X}$ . We increase  $\varepsilon$  gradually to see the evolution of  $\mathcal{T}_\varepsilon(\mathbf{X})$ . If we consider  $\varepsilon$  as the spatial resolution to view the shape of  $\mathbf{X}$ , the representative topological structures should be the structures appear in  $\mathcal{T}_\varepsilon(\mathbf{X})$  at the long-range of  $\varepsilon$ .

We illustrate this idea in Fig. 1 where we consider  $\mathbf{X}$  sampled from a figure-of-eight shape in two-dimensional space. First, we focus on the appearance and disappearance of loop-like structures. We can obtain the information of loops  $\Omega_1$  and  $\Omega_2$  by recording the values of  $\varepsilon$  where each loop appears then disappears. Similarly, number of connected components in  $\mathcal{T}_\varepsilon(\mathbf{X})$  is equal to number of points in  $\mathbf{X}$  for sufficiently small  $\varepsilon$ , but all of them are merged into one component for sufficiently large  $\varepsilon$ . Generally, we can track the emergent and vanishment of topological structures such as connected components, loops, and cavities over the evolution of  $\mathcal{T}_\varepsilon(\mathbf{X})$  [50]. We assign to each structure of them, a pair called *persistence pair*  $(b, d)$ , where the structure appears at  $\varepsilon = b$  and disappears at  $\varepsilon = d$ . We call  $b$  and  $d$  as *birth-scale* and *death-scale* of the structure with the *lifetime* as  $d - b$ . In the computational routine, the evolution of  $\mathcal{T}_\varepsilon(\mathbf{X})$  is modeled by a sequence of nested geometrical objects called filtration [50, 51]. The output of persistent homology, which we consider as the *topological features* to represent the shape of  $\mathbf{X}$ , is the collection of persistence pairs for all connected components, loops, and generally, holes in the constructed filtration. Topological features are repre-

sented as a two-dimensional diagram of multiset points, called *persistence diagram*, where each point denotes a persistence pair. We present the definition of filtration, holes, and illustration of the persistence diagram in the Supplemental Material [50].

*Unsupervised topological persistence scheme.*— Many statistical-learning algorithms require an inner product between the data in the vector form. However, the space of persistence diagrams is not a vector space. To address this problem, we use the kernel technique, which maps the topological features to a space called *kernel-mapped feature space* where we can define the inner product [46, 52–54]. Consider a collection  $\mathcal{D} = \{D_1, D_2, \dots, D_M\}$  of persistence diagrams, a kernel function  $K : \mathcal{D} \times \mathcal{D} \rightarrow \mathbb{R}$  is defined such that the matrix  $G$  with size  $M \times M$  and its elements  $g_{ij} = K(D_i, D_j)$ , called the Gram matrix is symmetric and positive definite. Then the Gram matrix can be fed to unsupervised learning algorithms such as nonlinear dimensional reduction or spectral clustering methods [55–57]. We employ the method in Ref. [54], which relies upon the Fisher information geometry to construct the kernel.

We demonstrate the usefulness of topological features in detecting the topological phase transition in the two-dimensional XY model. Topological phase transition is a fundamental class of phase transitions that do not possess the onset of a symmetry-breaking phase in the physical system. We consider the classical two-dimensional XY model described by the energy configuration  $E\{\theta_i\} = -J \sum_{\langle i,j \rangle} \cos(\theta_i - \theta_j)$ , where  $\theta_i$  is the angle of the XY spin at site  $i$  on the square lattice. The sum is over all the nearest-neighbor pairs in the lattice sites and  $J$  is the exchange interaction between spins. The topological phases are characterized by the formation of particular stable structures such as vortices or antivortices in the spin configuration. This model exhibits the topological phase transition, so called BKT phase transition at the critical temperature  $(T/J)_{\text{BKT}} \simeq 0.89$ . This phase transition has been explored in both supervised [22] and unsupervised [11–14, 24] schemes but lacking of the interpretability for the topological aspects of spin configurations.

To feed the data to our topological persistence machine, we use spin configurations on a square lattice with  $N = 32 \times 32$  sites, governed by the thermal distribution  $\rho(\{\theta_i\}) \propto e^{-E\{\theta_i\}/k_B T}$ , where  $k_B$  is the Boltzmann constant. We set  $k_B = 1$ ,  $J = 1$ , and initialize 10 initial configurations for each temperature  $T$ . We use Metropolis algorithm to bring the initial configuration into a thermodynamic equilibrium state. We explore the topological features of a set  $\mathbf{P}$  of points  $\mathbf{p}_i = (x_i, y_i, \cos(\theta_i), \sin(\theta_i))$ , where  $x_i, y_i$ , and  $\theta_i$  are the  $x$ -coordinate,  $y$ -coordinate, and the angle of the XY spin at site  $i$  on the square lattice. We introduce the distance between sites  $i$  and  $j$  as  $\xi \sqrt{(x_i - x_j)^2 + (y_i - y_j)^2} + (1 - \xi) \sqrt{2[1 - \cos(\theta_i - \theta_j)]}$ . Here,  $\xi$  is a positive rescaling coefficient introduced to

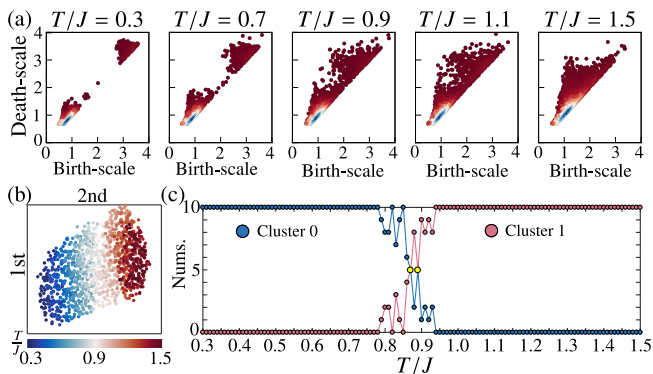


FIG. 2. (a) Persistence diagrams calculated from bare XY spin configurations. The blue and red parts correspond with high and low densities of points. (b) Nonlinear projection from the kernel-mapped feature space of the topological features to a two-dimensional display using UMAP [57]. (c) Detection of the topological phase transition using kernel spectral clustering [56]. The number of data grouped into each cluster versus temperature  $T/J$  is displayed.

adjust the scale different between the distance in the lattice and the distance induced by phase  $\theta_i$ . We set  $\xi = 0.5$  in our experiments. The topological phase transition is visualized clearly if we look at the persistence diagrams of loop structures aggregated by the value of  $T/J$  [Fig. 2(a)].

We demonstrate that our topological persistence machine can provide qualitative insights to explain the topological aspects before and after the transition. At low temperatures, a single vortex is difficult to exist alone in the spin configuration, then vortices pair up with antivortices, largely canceling out their effect. As a result, the spins throughout the two-dimension align to a certain degree of topological order. Then there are two major groups of loops in  $\mathbf{P}$ : a group of ordered spins, and a group of spins which form vortices. As illustrated in Fig. 2(a), for relatively low values of  $T/J$ , topological features are distributed in two major concentrated groups. At high values of  $T/J$ , vortices and antivortices are plentiful, and the spins are disordered. Loops with various sizes are generated, and the distribution of topological features becomes wider.

Next, we present the unsupervised method to detect BKT phase transition. We compute Gram matrix of persistence diagrams of loops corresponding with  $T/J = 0.30, 0.31, \dots, 1.50$ . We use UMAP [57], which is a nonlinear dimensionality reduction technique to project from the kernel-mapped feature space of diagrams into a two-dimensional display [Fig. 2(b)]. Here, points appear to be distinguishable in low- and high-temperature regimes with the transition region at  $T/J = 0.8 \sim 1.0$ . Figure 2(c) presents the result of the kernel spectral clustering method [56] based on Gram matrix to cluster the spin configurations into two clusters. Here, blue and

red points represent the number of configurations belong to each cluster in each value of  $T/J$ . It is clearly clustered into low- and high-temperature regimes except at the temperature around  $T/J = 0.9 \pm 0.1$ . The transition (yellow points) in the proportion of number configurations belong to each cluster is at temperature  $T/J \simeq 0.89$ , which agrees with the known phase transition point  $(T/J)_{\text{BKT}} \simeq 0.89$ . Note that our method can detect this transition without prior labeling or prior knowledge of topological phases.

*Topological persistence complexity*—The kernel method of topological features provides a useful way to determine the differences in the topological structures and can be fed easily into machine learning contexts. However, to directly quantify the complexity of states based on topological features, we can work with more global forms of featurization, namely, point summaries of a given persistence diagram. Here, we employ two types of point summaries and consider them as complexity measures to study the phase of matters.

The first complexity measure is the  $p$ -norm  $\mathcal{P}_p$  of lifetimes of topological features, which is a stable point summary of persistence diagram  $D$  defined as [58]:

$$\mathcal{P}_p(D) = \left[ \sum_{(b,d) \in D} |d-b|^p \right]^{1/p}. \quad (1)$$

$\mathcal{P}_\infty(D)$  captures the topological feature having maximum lifetime, and  $\mathcal{P}_2(D)$  represents the Euclidean distance of points in  $D$  to the diagonal. The second complexity measure is the normalized entropy from the lifetimes of topological features [59]:

$$\mathcal{E}(D) = -\frac{1}{\log_2 \mathcal{S}(D)} \sum_{(b,d) \in D} \frac{|d-b|}{\mathcal{S}(D)} \log_2 \left( \frac{|d-b|}{\mathcal{S}(D)} \right), \quad (2)$$

where  $\mathcal{S}(D) = \sum_{(b,d) \in D} |d-b|$  is the sum of lifetimes in the diagram  $D$ .  $\mathcal{P}_p(D)$  and  $\mathcal{E}(D)$  can be used as meaningful measures of complexity such as disorder in distances and mutual interactions between bodies in the system. We show that these complexity measures can be used to estimate quantum phase transitions, which are often characterized by quantum averages over physical observables such as two-point correlators. Here, we consider two standard workhorses of quantum many-body lattice physics, i.e., the transverse Ising model and the Bose-Hubbard model in 1D lattice.

The one-dimensional transverse Ising model consists of a chain of qubits (effective spin-1/2 particles) with Hamiltonian parameterized as  $\hat{H}_1 = -J_n \sum_{j=1}^{L-1} \hat{\sigma}_j^z \hat{\sigma}_{j+1}^z - J_n g \sum_{j=1}^L \hat{\sigma}_j^x$ . Here,  $\hat{\sigma}_j^\gamma$  ( $\gamma \in \{x, y, z\}$ ) is the Pauli operator to measure the spin along the  $\gamma$  direction of the Bloch sphere,  $J_n$  is nearest-neighbour coupling parameter, and  $g$  is transverse field parameter. For  $g \ll 1$ , the nearest-neighbor coupling

term dominates; therefore, all spins tend to be completely aligned in the up or down direction in the ground state. For  $g \gg 1$ , the external field dominates, and all spins in the ground state are aligned with the external field. The quantum phase transition at the critical point  $g_c = 1$  is evidenced by a change in the long-range behavior of the two points correlator.

The one-dimensional Bose Hubbard model takes the form  $\hat{H}_B = -t \sum_{i=1}^{L-1} (\hat{b}_i^\dagger \hat{b}_{i+1} + \hat{b}_{i+1}^\dagger \hat{b}_i) + \frac{U}{2} \sum_{i=1}^L \hat{n}_i (\hat{n}_i - 1) - \mu \sum_{i=1}^L \hat{n}_i$ , where  $[\hat{b}_i, \hat{b}_j^\dagger] = \delta_{ij}$ . Here,  $\hat{b}_i$  and  $\hat{b}_i^\dagger$  are bosonic annihilation and creation operators,  $\hat{n}_i = \hat{b}_i^\dagger \hat{b}_i$  is the number of particles on site  $i$ , and  $t$  is the tunneling parameter which are suppressed by on-site particle interaction  $U$ . The filling factor  $\bar{n} = \frac{1}{L} \sum_{i=1}^L \langle \hat{n}_i \rangle$  is controlled by the chemical potential  $\mu$ . For commensurate filling such as unit filling  $\bar{n} = 1$ , the model exhibits the BKT transition in the limit  $L \rightarrow \infty$ , while for small  $L$ , the effective critical point can occur at a ratio  $(t/U)_{\text{BKT}} \approx 0.2$  [60].

We use matrix product state (MPS) [61] method implemented in OpenMPS library [62–64] to simulate these models. Here, we employ the same setting of convergence parameters from Ref. [65]. Given the ground state  $|\psi\rangle$  obtained from the simulation, the density matrix  $\rho$  is calculated as  $\rho = |\psi\rangle \langle \psi|$ . To obtain the persistence diagrams, we need to define the distance between two sites on the lattice. Motivated from Ref. [65], first, we define quantum mutual information matrix  $\mathcal{M}$  whose elements  $\mathcal{M}_{ij} = \frac{1}{2}(S_i + S_j - S_{ij})$  for  $i \neq j$  and  $\mathcal{M}_{ii} = 0$ . Here,  $S_i = \text{Tr}(\hat{\rho}_i \log \hat{\rho}_i)$  and  $S_{ij} = -\text{Tr}(\hat{\rho}_{ij} \log \hat{\rho}_{ij})$  are the one and two point von Neumann entropies constructed from reduced density operators  $\hat{\rho}_i = \text{Tr}_{k \neq i} \hat{\rho}$  and  $\hat{\rho}_{ij} = \text{Tr}_{k \neq i, j} \hat{\rho}$ . Next, we define the distance between two sites  $i, j$  in the lattice as  $d_{ij} = \sqrt{1 - r_{ij}^2}$  [66], where  $r_{ij}$  is the Pearson correlation coefficient constructed from  $\mathcal{M}$

$$r_{ij} = \frac{\sum_{k=1}^L (\mathcal{M}_{ik} - \langle \mathcal{M}_i \rangle) (\mathcal{M}_{jk} - \langle \mathcal{M}_j \rangle)}{\sqrt{\sum_{k=1}^L (\mathcal{M}_{ik} - \langle \mathcal{M}_i \rangle)^2} \sqrt{\sum_{k=1}^L (\mathcal{M}_{jk} - \langle \mathcal{M}_j \rangle)^2}}. \quad (3)$$

Here,  $\langle \mathcal{M}_i \rangle$  is the average of  $\mathcal{M}_{ij}$  over  $j$ . We can think the sites on the lattice are placed in a high dimensional space associated with this distance function. Then we can calculate persistence diagrams for topological structures such as connected components and loops appear in the space. We show that quantifying complexity measures such as  $\mathcal{P}_p$  and  $\mathcal{E}$  can highlight different physical aspects of quantum phase and provide estimation for quantum critical points.

Figure 3 shows a finite size scaling study of complexity measures  $\mathcal{P}_2$  and  $\mathcal{E}$  in the transverse Ising model for the persistence diagrams of connected components. We use min-max normalization as  $\mathcal{P}_2 \rightarrow \tilde{\mathcal{P}}_2$  and  $\mathcal{E} \rightarrow \tilde{\mathcal{E}}$  to normalize to unity for display on a single plot. These measure are clearly able to identify phase transitions in

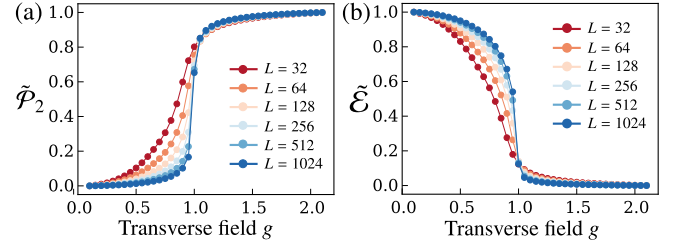


FIG. 3. Complexity measures based on persistent diagrams of connected components for transverse Ising model. (a) The 2-norm  $\mathcal{P}_2$  identifies the short range correlations of the paramagnetic ground state. (b) The normalized entropy  $\mathcal{E}$  serves as order parameter for the ferromagnetic phase. All of these measures have been min-max normalized for display on a single plot as  $\mathcal{P}_2 \rightarrow \tilde{\mathcal{P}}_2$ ,  $\mathcal{E} \rightarrow \tilde{\mathcal{E}}$ .

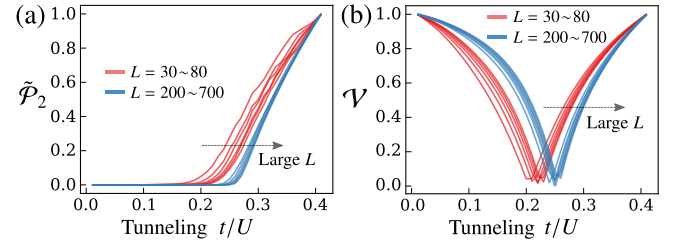


FIG. 4. Complexity measures based on persistent diagrams for Bose-Hubbard model. (a) The normalized 2-norm of loops. (b) The difference  $\mathcal{V}$  between normalized 2-norm and normalized entropy of connected components. The effective critical points are defined as parameters  $t/U$  to achieve  $\mathcal{V} = 0$ .

the transverse Ising model. The quantum critical point is sharp at  $g_c \approx 1$  when  $L \rightarrow \infty$ . Note that  $\mathcal{P}_2$  is low in the ferromagnetic phase where the distance  $d_{ij}$  approximates zero since sites are strongly mutated and the sequences of quantum mutual information  $\{\mathcal{M}_{ik}\}_{k=1, \dots, N}$  and  $\{\mathcal{M}_{jk}\}_{k=1, \dots, N}$  display a strong linear relationship. Therefore, the lifetimes of connected components approximately take the same values, and the normalized entropy is high. In the paramagnetic phase, due to the exponential decay of correlations, sites exhibit more tightly bound to their nearest neighbors compare to others. Sites are considered to be divided into clusters in a high dimensional space with different scales of distances, thus  $\mathcal{P}_2$  is high and  $\mathcal{E}$  is low in paramagnetic phase.

In Fig. 4(a) we observe the clear transition of  $\mathcal{P}_2$  of loops constructed from Bose-Hubbard model. For small system size, we can consider these transition points as effective critical point of quantum system. Since  $\mathcal{P}_2$  displays the scale of spatial quantum correlation,  $\mathcal{E}$  serves as order parameters, we define another complexity measure to evaluate the balance of  $\mathcal{P}_2$  and  $\mathcal{E}$  as  $\mathcal{V} = |\mathcal{E} - \tilde{\mathcal{P}}_2|$ . We define the effective critical point at parameter  $(t/U)_e$  to achieve the intriguing point  $\mathcal{V} = 0$ . Figure 4(b) demonstrates the value of  $\mathcal{V}$  calculated from persistence diagrams of connected components, and effective criti-

cal points at different sizes of system as  $L = 30 \sim 70$  (red lines) and  $L = 200 \sim 700$  (blue lines). The BKT transition of Bose–Hubbard model in 1D lattice occurs for very large  $L$ , with the recent estimation using the density-matrix renormalization group as  $(t/U)_{\text{BKT}} = 0.29 \pm 0.01$  [67] and  $(t/U)_{\text{BKT}} = 0.305$  [68, 69], or by using network measures from quantum mutual information [65]. Interestingly, the BKT transition can be also quantitatively obtained from our method by fitting power laws of the curve  $(t/U)_e(L) = (t/U)_{\text{BKT}} + \alpha L^{-\beta}$  for effective critical points. Here, using data in Fig. 4(b), we can obtain  $(t/U)_{\text{BKT}} = 0.289 \pm 0.001$ ,  $\alpha = -0.234 \pm 0.001$ ,  $\beta = 0.300 \pm 0.008$ . We note that this BKT transition is estimated without investigating an extremely large system or having prior knowledge about the decay correlation.

*Conclusions.*— Our approach produces the quantitative topological features of raw data of physical states. These features can be useful to identify the phases of matter with proper interpretations. This work opens up new possibilities for exploring the phase transitions in physical systems without requiring prior knowledge. Such possibilities include application to unravel complex phase diagrams of general experimental systems, where the Hamiltonian might not be known, and traditional physical measures are weakly applicable.

---

\* zoro@biom.t.u-tokyo.ac.jp

† mark@biom.t.u-tokyo.ac.jp

‡ hasegawa@biom.t.u-tokyo.ac.jp

- [1] L. v. d. Maaten and G. Hinton, *J. Mach. Learn. Res.* **9**, 2579 (2008).
- [2] R. R. Coifman, S. Lafon, A. B. Lee, M. Maggioni, B. Nadler, F. Warner, and S. W. Zucker, *Proc. Natl. Acad. Sci. USA* **102**, 7426 (2005).
- [3] B. Nadler, S. Lafon, I. Kevrekidis, and R. R. Coifman, in *Advances in Neural Information Processing Systems 18*, edited by B. S. Yair Weiss and J. Platt (MIT Press, 2006) pp. 955–962.
- [4] J. Carrasquilla and R. G. Melko, *Nat. Phys.* **13**, 431 (2017).
- [5] K. Ch’ng, J. Carrasquilla, R. G. Melko, and E. Khatami, *Phys. Rev. X* **7**, 031038 (2017).
- [6] Y. Zhang and E.-A. Kim, *Phys. Rev. Lett.* **118**, 216401 (2017).
- [7] Y. Zhang, R. G. Melko, and E.-A. Kim, *Phys. Rev. B* **96**, 245119 (2017).
- [8] E. P. Van Nieuwenburg, Y.-H. Liu, and S. D. Huber, *Nature Physics* **13**, 435 (2017).
- [9] T. Ohtsuki and T. Ohtsuki, *J. Phys. Soc. Jpn.* **85**, 123706 (2016).
- [10] T. Ohtsuki and T. Ohtsuki, *J. Phys. Soc. Jpn.* **86**, 044708 (2017).
- [11] W. Hu, R. R. P. Singh, and R. T. Scalettar, *Phys. Rev. E* **95**, 062122 (2017).
- [12] S. J. Wetzel, *Phys. Rev. E* **96**, 022140 (2017).
- [13] C. Wang and H. Zhai, *Phys. Rev. B* **96**, 144432 (2017).
- [14] C. Wang and H. Zhai, *Front. Phys.* **13**, 130507 (2018).
- [15] N. Yoshioka, Y. Akagi, and H. Katsura, *Phys. Rev. B* **97**, 205110 (2018).
- [16] P. Zhang, H. Shen, and H. Zhai, *Phys. Rev. Lett.* **120**, 066401 (2018).
- [17] D. Carvalho, N. A. García-Martínez, J. L. Lado, and J. Fernández-Rossier, *Phys. Rev. B* **97**, 115453 (2018).
- [18] P. Huembeli, A. Dauphin, and P. Wittek, *Phys. Rev. B* **97**, 134109 (2018).
- [19] I. A. Iakovlev, O. M. Sotnikov, and V. V. Mazurenko, *Phys. Rev. B* **98**, 174411 (2018).
- [20] R. A. Vargas-Hernández, J. Sous, M. Berciu, and R. V. Krems, *Phys. Rev. Lett.* **121**, 255702 (2018).
- [21] M. J. S. Beach, A. Golubeva, and R. G. Melko, *Phys. Rev. B* **97**, 045207 (2018).
- [22] P. Suchsland and S. Wessel, *Phys. Rev. B* **97**, 174435 (2018).
- [23] K. Ch’ng, N. Vazquez, and E. Khatami, *Phys. Rev. E* **97**, 013306 (2018).
- [24] J. F. Rodríguez-Nieva and M. S. Scheurer, *Nat. Phys.* , 1 (2019).
- [25] W. Zhang, J. Liu, and T.-C. Wei, *Phys. Rev. E* **99**, 032142 (2019).
- [26] Y. Ming, C.-T. Lin, S. D. Bartlett, and W.-W. Zhang, *Npj Comput. Mater.* **5**, 1 (2019).
- [27] B. S. Rem, N. Käming, M. Tarnowski, L. Asteria, N. Fläschner, C. Becker, K. Sengstock, and C. Weitenberg, *Nat. Phys.* **15**, 917 (2019).
- [28] G. Carleo, I. Cirac, K. Cranmer, L. Daudet, M. Schuld, N. Tishby, L. Vogt-Maranto, and L. Zdeborová, *Rev. Mod. Phys.* **91**, 045002 (2019).
- [29] G. Carlsson, *Bull. Amer. Math. Soc.* **46**, 255 (2009).
- [30] M. Kramar, A. Goulet, L. Kondic, and K. Mischaikow, *Phys. Rev. E* **87**, 042207 (2013).
- [31] S. Ardanza-Trevijano, I. Zuriguel, R. Arévalo, and D. Maza, *Phys. Rev. E* **89**, 052212 (2014).
- [32] M. Kramár, A. Goulet, L. Kondic, and K. Mischaikow, *Phys. Rev. E* **90**, 052203 (2014).
- [33] T. Nakamura, Y. Hiraoka, A. Hirata, E. G. Escolar, and Y. Nishiura, *Nanotechnology* **26**, 304001 (2015).
- [34] Y. Hiraoka, T. Nakamura, A. Hirata, E. G. Escolar, K. Matsue, and Y. Nishiura, *Proc. Natl. Acad. Sci. USA* **113**, 7035 (2016).
- [35] T. Ichinomiya, I. Obayashi, and Y. Hiraoka, *Phys. Rev. E* **95**, 012504 (2017).
- [36] T. Takahashi, A. H. Clark, T. Majmudar, and L. Kondic, *Phys. Rev. E* **97**, 012906 (2018).
- [37] D. Taylor, F. Klimm, H. A. Harrington, M. Kramár, K. Mischaikow, M. A. Porter, and P. J. Mucha, *Nat. Commun.* **6**, 7723 (2015).
- [38] S. Maletić, Y. Zhao, and M. Rajković, *Chaos* **26**, 053105 (2016).
- [39] I. Donato, M. Gori, M. Pettini, G. Petri, S. De Nigris, R. Franzosi, and F. Vaccarino, *Phys. Rev. E* **93**, 052138 (2016).
- [40] K. Mittal and S. Gupta, *Chaos* **27**, 051102 (2017).
- [41] M. Sinhuber and N. T. Ouellette, *Phys. Rev. Lett.* **119**, 178003 (2017).
- [42] L. Speidel, H. A. Harrington, S. J. Chapman, and M. A. Porter, *Phys. Rev. E* **98**, 012318 (2018).
- [43] Q. H. Tran and Y. Hasegawa, *Phys. Rev. E* **99**, 032209 (2019).
- [44] Q. H. Tran, V. T. Vo, and Y. Hasegawa, *Phys. Rev. E* **100**, 032308 (2019).
- [45] A. Myers, E. Munch, and F. A. Khasawneh, *Phys. Rev.*

- E **100**, 022314 (2019).
- [46] G. Kusano, Y. Hiraoka, and K. Fukumizu, in *Proceedings of The 33rd International Conference on Machine Learning*, Proceedings of Machine Learning Research, Vol. 48, edited by M. F. Balcan and K. Q. Weinberger (PMLR, New York, New York, USA, 2016) pp. 2004–2013.
- [47] H. Edelsbrunner, D. Letscher, and A. Zomorodian, *Discrete Comput. Geom.* **28**, 511 (2002).
- [48] A. Zomorodian and G. Carlsson, *Discrete Comput. Geom.* **33**, 249 (2005).
- [49] H. Edelsbrunner and J. Harer, *Computational Topology. An Introduction* (American Mathematical Society, Providence, RI, 2010).
- [50] See Supplemental Material.
- [51] T. Kaczynski, K. Mischaikow, and M. Mrozek, *Computational homology*, Vol. 157 (Springer, 2006).
- [52] J. Reininghaus, S. Huber, U. Bauer, and R. Kwitt, in *Proceedings of the 28th IEEE Conference on Computer Vision and Pattern Recognition* (IEEE, Boston, MA, USA, 2015) pp. 4741–4748.
- [53] M. Carrière, M. Cuturi, and S. Oudot, in *Proceedings of the 34th International Conference on Machine Learning*, Proceedings of Machine Learning Research, Vol. 70, edited by D. Precup and Y. W. Teh (PMLR, International Convention Centre, Sydney, Australia, 2017) pp. 664–673.
- [54] T. Le and M. Yamada, in *Proceedings of the 32nd International Conference on Neural Information Processing Systems*, NIPS’18 (Curran Associates Inc., USA, 2018) pp. 10028–10039.
- [55] B. Schölkopf, A. Smola, and K.-R. Müller, *Neural Comput.* **10**, 1299 (1998).
- [56] N. Cristianini, J. Shawe-Taylor, and J. S. Kandola, in *Advances in Neural Information Processing Systems 14*, edited by T. G. Dietterich, S. Becker, and Z. Ghahramani (MIT Press, 2002) pp. 649–655.
- [57] L. McInnes, J. Healy, and J. Melville, [Preprint at arXiv:1802.03426](https://arxiv.org/abs/1802.03426) (2018).
- [58] D. Cohen-Steiner, H. Edelsbrunner, J. Harer, and Y. Mileyko, *Found. Comput. Math.* **10**, 127 (2010).
- [59] H. Chintakunta, T. Gentimis, R. Gonzalez-Diaz, M.-J. Jimenez, and H. Krim, *Pattern Recognition* **48**, 391 (2015).
- [60] L. D. Carr, M. L. Wall, D. G. Schirmer, R. C. Brown, J. E. Williams, and C. W. Clark, *Phys. Rev. A* **81**, 013613 (2010).
- [61] U. Schollwck, *Annals of Physics* **326**, 96 (2011).
- [62] M. L. Wall and L. D. Carr, *New J. Phys.* **14**, 125015 (2012).
- [63] D. Jaschke, M. L. Wall, and L. D. Carr, *Computer Physics Communications* **225**, 59 (2018).
- [64] Matrix product state open source code. <https://sourceforge.net/projects/openmps/>.
- [65] M. A. Valdez, D. Jaschke, D. L. Vargas, and L. D. Carr, *Phys. Rev. Lett.* **119**, 225301 (2017).
- [66] V. Solo, [Preprint at arXiv:1908.06029](https://arxiv.org/abs/1908.06029) (2019).
- [67] T. D. Kühner, S. R. White, and H. Monien, *Phys. Rev. B* **61**, 12474 (2000).
- [68] S. Ejima, H. Fehske, and F. Gebhard, *EPL* **93**, 30002 (2011).
- [69] J. Carrasquilla, S. R. Manmana, and M. Rigol, *Phys. Rev. A* **87**, 043606 (2013).

# Supplemental Material for “Topological Persistence Machine of Phase Transitions”

Quoc Hoan Tran, Mark Chen and Yoshihiko Hasegawa

This supplementary material describes in detail the calculations, the experiments introduced in the main text, and the additional figures. Equation, figure and table numbers in this section are prefixed with S (e.g., Eq. (S1) or Fig. S1, Table S1). Numbers without the prefix (e.g., Eq. (1) or Fig. 1, Table 1) refer to items in the main text.

## 1 Persistent homology and topological features of data

In this section, we describe the primitive strategy for studying data using persistent homology. The mathematical background and preliminaries in detail can be found in Ref. [1].

### 1.1 Topological cover and topological features of data

We consider a data set  $\mathbf{X}$  of discrete points sampled from an unknown space as the subspace of the metric space  $(\mathbb{X}, d)$  with  $d$  denotes the distance defined on  $\mathbb{X} \times \mathbb{X}$ . Topological data analysis (TDA) aims to infer the topological properties of the underlying space of  $\mathbf{X}$  such as the number of connected components, loops, tunnels, and cavities, etc. However, if we only consider discrete points in  $\mathbf{X}$ , there are  $|\mathbf{X}|$  connected components without any loop, tunnel, or cavity, and therefore no information about the topological properties of the underlying space. The idea of TDA is to study the topological properties via the *topological cover* of  $\mathbf{X}$ . Here, given a nonnegative proximity parameter  $\varepsilon$ , the  $\varepsilon$ -scale topological cover  $\mathcal{T}_\varepsilon(\mathbf{X})$  of  $\mathbf{X}$  is defined as the set of all points in  $\mathbb{X}$  within distance  $\varepsilon/2$  from some point in  $\mathbf{X}$ .

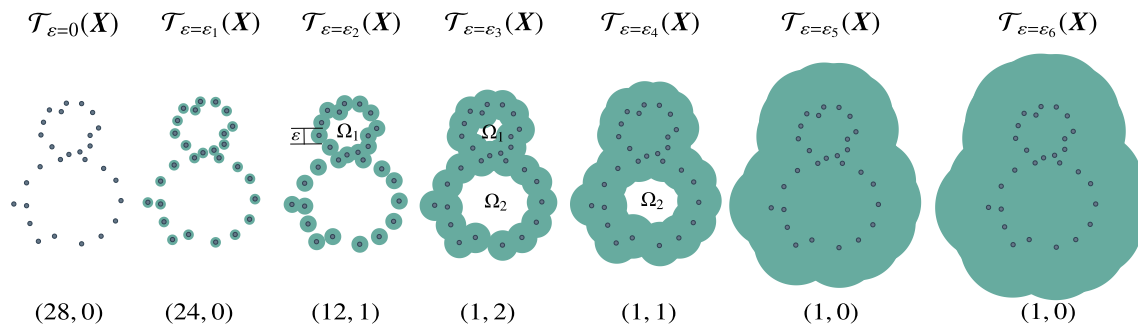


FIG. S1. Exemplary of an evolution of topological covers  $\mathcal{T}_\varepsilon(\mathbf{X})$  constructed from the data set  $\mathbf{X}$ . Topological structure changes are tracked, such as the merging of connected components, and the emergence and disappearance of loops present in the space with increasing  $\varepsilon$ . For instance, the loop  $\Omega_1$  appears at  $\varepsilon = \varepsilon_2$  then disappears at  $\varepsilon = \varepsilon_4$ , whereas the loop  $\Omega_2$  appears at  $\varepsilon = \varepsilon_3$  then disappears at  $\varepsilon = \varepsilon_5$ . For each  $\varepsilon$ , the number of connected components and the number of loops are listed underneath.

If data is noisy and lies in a high-dimensional space, this strategy must deal with several critical shortcomings. First, the topological properties of  $\mathcal{T}_\varepsilon(\mathbf{X})$  are not robust to noise in  $\mathbf{X}$ . Second, the selection of  $\varepsilon$  is a very sensitive problem, especially when the high-dimensional data cannot be visualized directly. To deal with the above-mentioned problems, the key idea behind persistent homology is to consider the topological properties of the entire family  $\mathcal{T}_\varepsilon(\mathbf{X})$  as  $\varepsilon$  varies. If we consider  $\varepsilon$  as the spatial resolution to view  $\mathbf{X}$ , the representative topological structures in the underlying space of  $\mathbf{X}$  should be the structures appear at different resolutions. We illustrate this idea in Fig. S1 when we consider  $\mathbf{X}$  sampled from the shape of the number “8” in two-dimensional space. Now, starting with  $\varepsilon = 0$ , the topological cover

$\mathcal{T}_{\varepsilon=0}(\mathbf{X})$  contains only the discrete points in  $\mathbf{X}$ . As  $\varepsilon$  increases, connections exist between components in  $\mathcal{T}_{\varepsilon}(\mathbf{X})$ , enabling us to obtain an evolution topological covers in the space. Moreover, if  $\varepsilon$  becomes considerably large, all the components get connected with each other, we obtain a large and overlapped cover whereby no useful information can be conveyed.

Persistent homology tracks the variation of topological structures, i.e., connected components, and holes over the evolution of topological covers (see the next subsection for the definition of holes). For instance, if we focus on the appearance and disappearance of loop-like structures in Fig. S1, we can obtain the information of two loops  $\Omega_1$  and  $\Omega_2$ . The loop  $\Omega_1$  appears at  $\varepsilon = \varepsilon_2$  then disappears at  $\varepsilon = \varepsilon_4$ , whereas the loop  $\Omega_2$  appears at  $\varepsilon = \varepsilon_3$  then disappears at  $\varepsilon = \varepsilon_5$ . We can distinguish loops if we assign to each loop  $\Omega$  in the evolution a pair of scale called *persistence pair*  $(b, d)$ , where at  $\varepsilon = b$ , the loop  $\Omega$  appears, and at  $\varepsilon = d$ ,  $\Omega$  disappears. We call  $b$  and  $d$  as *birth-scale* and *death-scale* of loop  $\Omega$ . The difference between *death-scale* and *birth-scale*, i.e.,  $|d - b|$ , tells us about the magnitude of the loop  $\Omega$  in the space, or the *lifetime* of the loop. We also obtain the persistence pairs for connected components appear first at  $\mathcal{T}_{\varepsilon=0}(\mathbf{X})$  and are merged together along with the evolution of topological covers.

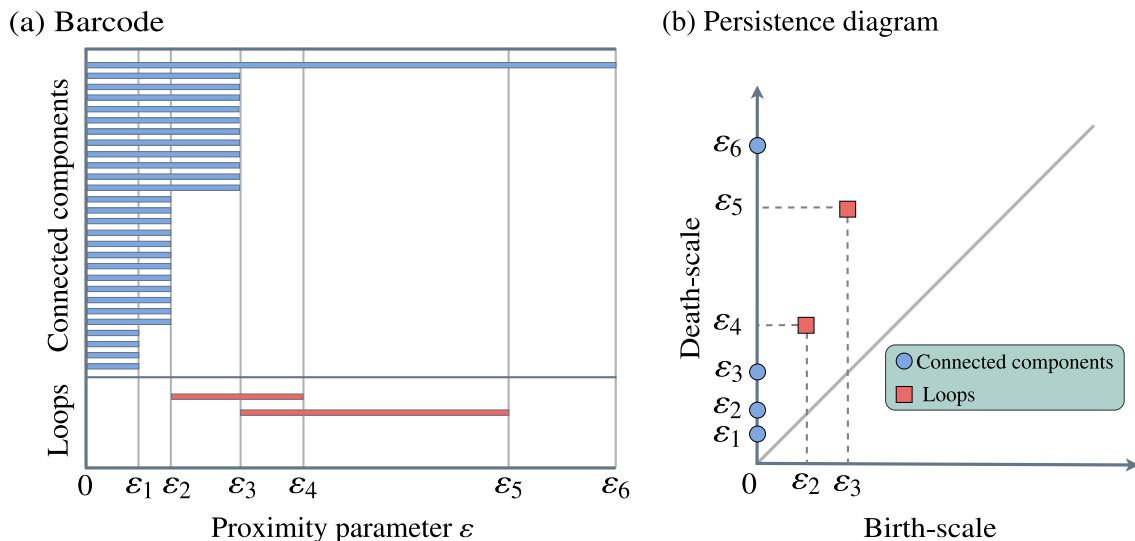


FIG. S2. The visualization for the output of persistent homology for the evolution of topological covers in Fig. S1. Each connected component or each loop pattern in the filtration corresponds with a persistence pair  $(b, d)$  represented for the values of  $\varepsilon$  at the emergence (*birth-scale*,  $\varepsilon = b$ ) and the disappearance (*death-scale*,  $\varepsilon = d$ ) of the pattern. Each bar begins at the value of the birth-scale, then ends at the value of the death-scale in a persistence pair. The collection of these bars is called a *barcode*, and the representation of all persistence pairs in a two-dimensional diagram (connected components in blue circles and loops in red circles) is called a *persistence diagram*. (a) Barcode and (b) Persistence diagram for the evolution of topological covers in Fig. S1. Note that, points in the diagram are multi-set points.

The output of persistent homology, which we consider as the *topological features* to represent the shape of data set  $\mathbf{X}$  is the collection of persistence pairs for all connected components, loops, and generally, holes in the evolution of topological covers  $\mathcal{T}_{\varepsilon}(\mathbf{X})$ . For example, the lifetime of these patterns are described as blue bars (for connected components) and red bars (for loops) in Fig. S2(a). Each bar begins at the value of the birth-scale, then ends at the value of the death-scale in a persistence pair. The collection of these bars is called a *barcode* of  $\mathbf{X}$ . Another representation of the topological features is a two-dimensional diagram of multiset points, a called *persistence diagram* [Fig. S2(b)]. In this diagram, each point denotes a persistence pair calculated from the evolution of topological covers.

## 1.2 Filtration of simplicial complex

In the computational routine, the evolution of  $\mathcal{T}_\varepsilon(\mathbf{X})$  is modeled by much more mathematically and computationally tractable representation called filtration. Filtration is a sequence of nested geometrical objects called simplicial complexes. Here, simplicial complexes are complexes of geometric structures called simplices. An  $n$ -simplex is a generalization of the notion of a triangle or tetrahedron to arbitrary dimensions. More precisely, an  $n$ -simplex is geometrically the convex hull of its  $n + 1$  affinely independent positioned vertices in the space. For example, a 0-simplex is a point, a 1-simplex is a line segment with two end points as its faces, a 2-simplex is a triangle together with its enclosed area with three edges and three vertices as its faces. Similarly, a 3-simplex is a filled tetrahedron with triangles, edges, and vertices as its faces, and a 4-simplex is beyond of visualization but it is a filled shape with tetrahedrons, triangles, edges, and vertices as its faces (Fig. S3). A simplicial complex is a collection of simplices, roughly formed when we “glue” together different simplices with a condition that the common parts of simplices in the simplicial complex must be the faces of both simplices (Fig. S4). We call a simplicial complex  $\mathcal{K}$  is a  $n$ -complex if  $n$  is the maximum number such that there is at least one  $n$ -simplex in  $\mathcal{K}$ .

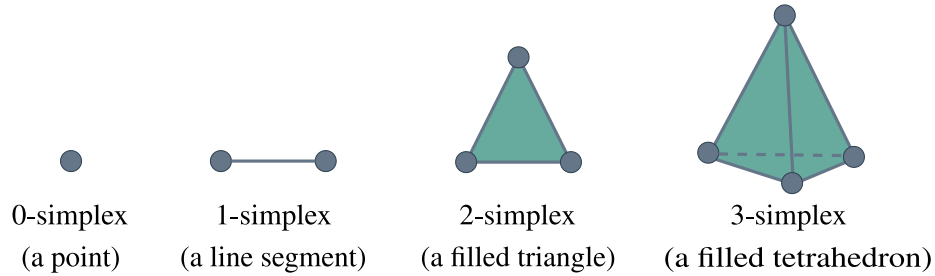


FIG. S3. A simplex is a generalization of the notion of a triangle or tetrahedron to arbitrary dimensions. For example, a 0-simplex is a point, a 1-simplex is a line segment, a 2-simplex is a triangle together with its enclosed area, and a 3-simplex is a filled tetrahedron, and so on.

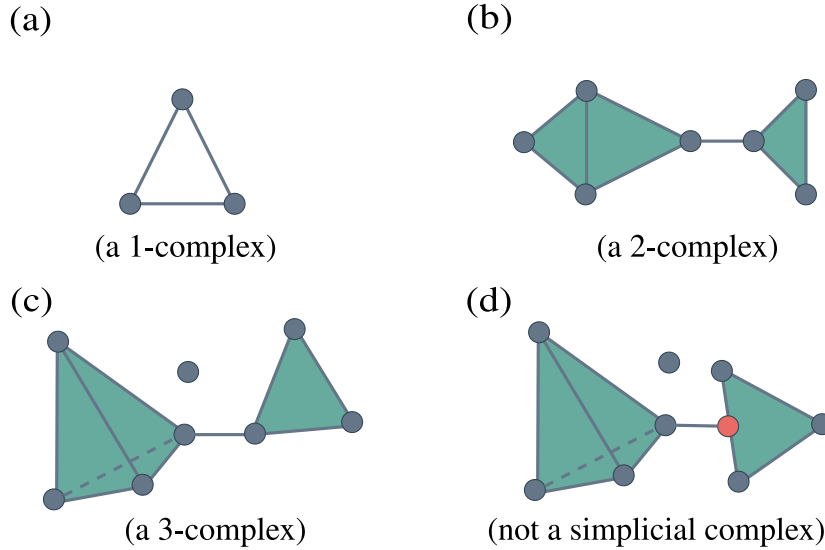


FIG. S4. A simplicial complex is a collection of simplices, such that the common parts of simplices in the simplicial complex must be the faces of both simplices. A simplicial complex  $\mathcal{K}$  is called a  $n$ -complex if  $n$  is the maximum number such that there is at least one  $n$ -simplex in  $\mathcal{K}$ . The illustration here depicts (a) a 1-complex, (b) a 2-complex, (c) a 3-complex, and (d) not a simplicial complex.

The next step is to construct a simplicial complex from  $\mathbf{X}$ . We focus on Vietoris–Rips complex model in this paper since it is the most practical and mainly used model from a computational view [2]. Given a nonnegative proximity parameter  $\varepsilon$ , the  $\varepsilon$ -scale Vietoris–Rips complex  $V_R(\mathbf{X}, \varepsilon)$  is a set of simplices such that every collection of  $n + 1$  affinely independent points in  $\mathbf{X}$  forms an  $n$ -simplex in  $V_R(\mathbf{X}, \varepsilon)$  if the pairwise distance between the points is less than or equal to  $\varepsilon$ . Intuitively, we can consider a union

of balls of radius  $\varepsilon/2$  centered at each point in  $\mathbf{X}$ , then each simplex is built over a subset of points if the balls intersect between every pair of points. In turn, the constructed complex  $V_R(\mathbf{X}, \varepsilon)$  provides information on the topological structure of  $\mathbf{X}$  associated with  $\varepsilon$ . Now, starting with  $\varepsilon = 0$ , the complex contains only the 0-simplices, i.e., the discrete points. As  $\varepsilon$  increases, connections exist between the points, enabling us to obtain a filtration, with edges (1-simplices), and filled triangles (2-simplices) are included into the complexes. Moreover, if  $\varepsilon$  becomes considerably large, all the points gets connected with each other, whereby no useful information can be conveyed (Fig. S5).

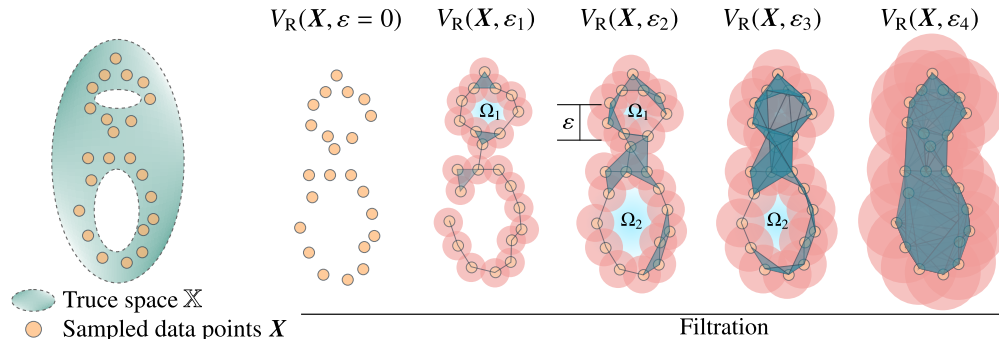


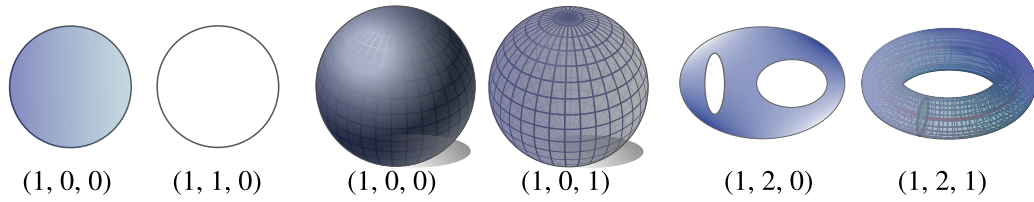
FIG. S5. The data set  $\mathbf{X}$  sampled from true but unknown space  $\mathbb{X}$  is transformed into a filtration of Vietoris–Rips complex  $V_R(\mathbf{X}, \varepsilon)$ .

### 1.3 Definition of holes

We remind that persistent homology tracks the variation of topological structures over the filtration. We refer to the topological structures, i.e., “holes”, as connected components, tunnels or loops (e.g., a circle of torus), cavities or voids (e.g., the space enclosed by a sphere), and so on. In persistent homology, a hole is identified via the cycle that surrounds it. In a given manifold, a cycle is a closed submanifold, and a boundary is a cycle that is also the boundary of a submanifold. Holes correspond to cycles that are not themselves boundaries. For instance, a disk is a two-dimensional surface with a one-dimensional boundary (i.e., a circle). If we puncture the disk, we obtain a one-dimensional hole that is enclosed by the circle, which is no longer a boundary. Similarly, a filled ball is a three-dimensional object with a two-dimensional boundary (i.e., a surface sphere). If we empty the inside of the ball, we obtain a two-dimensional hole that is enclosed by the surface sphere, which is no longer a boundary. Figure S6(a) shows some sample manifolds with the number of zero-, one-, and two-dimensional holes listed underneath.

Based on these observations, we can describe and classify holes in the simplicial complex according to the cycles that enclose holes. We define an  $n$ -chain as a collection of  $n$ -simplices in the complex. Therefore, in a simplicial complex, we can define an  $n$ -cycle as a closed  $n$ -chain and an  $n$ -boundary as an  $n$ -cycle, which is also the boundary of an  $(n + 1)$ -chain. Here, a 0-cycle is a connected component, a 1-cycle is a closed loop, and a 2-cycle is a shell. For instance, in Fig. S6(b), all loops  $A \rightarrow B \rightarrow D \rightarrow A$ ,  $B \rightarrow C \rightarrow D \rightarrow B$ , and  $A \rightarrow B \rightarrow C \rightarrow D \rightarrow A$  are 1-cycles because they are the closed collection of edges (1-simplices). Furthermore, the loop  $A \rightarrow B \rightarrow D \rightarrow A$  is a 1-boundary because it bounds a triangular face (2-simplex). An  $n$ -dimensional hole corresponds to an  $n$ -cycle that is not a boundary of any  $(n + 1)$ -chain in the simplicial complex. For instance, in Fig. S6(b), the loops  $B \rightarrow C \rightarrow D \rightarrow B$  and  $A \rightarrow B \rightarrow C \rightarrow D \rightarrow A$  characterize one-dimensional holes because these loops are 1-cycles but are themselves not 1-boundaries. Moreover, two  $n$ -cycles characterize the same hole when together they bound an  $(n + 1)$ -chain (i.e., their difference is an  $n$ -boundary). Intuitively, the connected components can be considered as zero-dimensional holes, the loops and tunnels as one-dimensional holes, and the cavities and voids as two-dimensional holes.

(a) Holes



(b) Simplicial complex

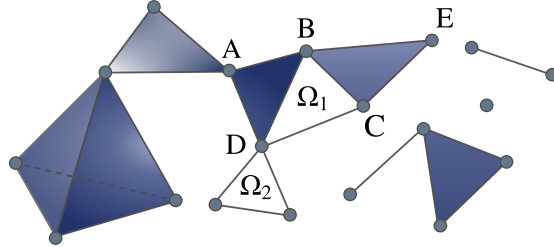


FIG. S6. (a) Sample manifolds with the number of zero-, one-, and two-dimensional holes listed underneath. Here, the connected component is a zero-dimensional hole. A one-dimensional hole is obtained by puncturing a disk. A two-dimensional hole is obtained by emptying the inside of a ball. (b) Example of a simplicial complex containing 19 points (0-simplices), 24 edges (1-simplices), eight triangular faces (2-simplices), and one filled tetrahedron (3-simplices). There are two one-dimensional holes  $\Omega_1$  and  $\Omega_2$  in this complex.

## References

- [1] Herbert Edelsbrunner and John Harer. *Computational Topology. An Introduction*. American Mathematical Society, Providence, RI, 2010.
- [2] Tomasz Kaczynski, Konstantin Mischaikow, and Marian Mrozek. *Computational homology*, volume 157. Springer, 2006.